ADVANCED FUNCTIONAL MATERIALS
www.afm-journal.de

Identification of Quaternary Shape Memory Alloys with Near-Zero Thermal Hysteresis and Unprecedented Functional Stability

By *Robert Zarnetta,* Ryota Takahashi, Marcus L. Young, Alan Savan, Yasubumi Furuya, Sigurd Thienhaus, Burkhard Maaß, Mustafa Rahim, Jan Frenzel, Hayo Brunken, Yong S. Chu, Vijay Srivastava, Richard D. James, Ichiro Takeuchi, Gunther Eggeler,* and *Alfred Ludwig*

Improving the functional stability of shape memory alloys (SMAs), which undergo a reversible martensitic transformation, is critical for their applications and remains a central research theme driving advances in shape memory technology. By using a thin-film composition-spread technique and high-throughput characterization methods, the lattice parameters of quaternary Ti–Ni–Cu–Pd SMAs and the thermal hysteresis are tailored. Novel alloys with near-zero thermal hysteresis, as predicted by the geometric non-linear theory of martensite, are identified. The thin-film results are successfully transferred to bulk materials and near-zero thermal hysteresis is observed for the phase transformation in bulk alloys using the temperature-dependent alternating current potential drop method. A universal behavior of hysteresis versus the middle eigenvalue of the transformation stretch matrix is observed for different alloy systems. Furthermore, significantly improved functional stability, investigated by thermal cycling using differential scanning calorimetry, is found for the quaternary bulk alloy $Ti_{50.2}Ni_{34.4}Cu_{12.3}Pd_{3.1}$.

1. Introduction

Within the class of materials showing a reversible martensitic phase transformation and a shape memory effect (SME), NiTi enjoys widespread and growing use in a variety of applications. Owing to its unique combination of properties: ductility, strength, corrosion resistance, biocompatibility, robust pseudoelasticity, and one- and two-way SME, it is commercially used in medical and actuator applications. Despite such attributes, there remain undesirable functional and structural fatigue properties of NiTi. Functional fatigue of shape memory alloys (SMAs) resulting in changes of physical, mechanical, and shape memory (SM) properties[1] during cyclic thermal or mechanical loading is related to irreversible processes, that is, generation of dislocations,[2,3] which take place during the martensitic phase transformation. Only recently, the mechanism for the multiplication of dislocations during martensitic transformations has been uncovered, based on transmission electron microscopy (TEM) investigations on single-crystal NiTi.[4] Accumulation of these defects eventually causes internal crack formation and growth, leading to catastrophic failure for many applications.[1,5]

The number of dislocations generated during the phase transformation is believed to be closely related to the geometric compatibility at the developing interface between austenite (high-temperature phase) and martensite (low-temperature phase). Due

[*] R. Zarnetta, Dr. M. L. Young, A. Savan, Dr. S. Thienhaus, B. Maaß, M. Rahim, Dr. J. Frenzel, H. Brunken, Prof. G. Eggeler, Prof. A. Ludwig
Institute for Materials
Ruhr-Universität Bochum
44780 Bochum (Germany)
E-mail: robert.zarnetta@rub.de

R. Zarnetta, Prof. G. Eggeler, Prof. A. Ludwig
Research Department Integrity of Small-Scale Systems/High-Temperature Materials (IS^3/HTM)
Ruhr-Universität Bochum
44780 Bochum (Germany)

Dr. R. Takahashi,[+] Prof. I. Takeuchi
Department of Materials Science and Engineering
University of Maryland
College Park, Maryland 20742 (USA)

Prof. Dr. Y.Furuya
Department of Intelligent Machines and Systems Engineering
Hirosaki University
Hirosaki 036-8561 (Japan)

Dr. Y. S.Chu[†]
Advanced Photon Source
Argonne National Laboratory
Argonne, IL 90439 (USA)

Dr. V. Srivastava, Prof. R. D. James
Department of Aerospace Engineering and Mechanics
University of Minnesota
Minneapolis, Minnesota 55455 (USA)

[+] Present address: Institute of Solid State Physics, University of Tokyo, 5-1-5 Kashiwanoha, Kashiwa, 277-8581 (Japan)

[†] Present address: National Synchrotron Light Source II, Brookhaven National Laboratory, Upton NY, 11973 (USA)

DOI: 10.1002/adfm.200902336

to this incompatibility, an elastic transition layer will form upon transformation, and both elastic energy and interfacial energy of the martensite twins will be stored. For some regimes of material parameters (elastic moduli, transformation strain, and twin-boundary energy) branching of the martensite becomes favorable and leads to a reduction of the total elastic plus interfacial energy at the austenite/martensite interface. In either case the fully developed austenite/martensite interface is associated with an energy barrier that must be overcome during the forward and reverse transformation, thus giving rise to transformation hysteresis.[6,7] The energy dissipation that occurs during the crossing of this barrier makes SMAs also useful as mechanical damping materials.[8]

As the transformation hysteresis can be correlated to the compatibility at the austenite/martensite interface and the compatibility itself to the fatigue properties, a direct correlation between transformation hysteresis and fatigue properties for SMA is expected. The correlation between large inherent transformation hysteresis and poor functional fatigue properties for SMAs cycled mechanically (pseudoelasticity)[9] or thermally (one-way SME)[10] has been well established. Thus, it is believed that the functional fatigue associated with the reversible martensitic phase transformation can be reduced by developing SMAs with extremely small transformation hysteresis.

In this paper, we demonstrate for the first time a targeted combinatorial thin-film search within a quaternary SMA thin film system for which high-throughput measurements of thermal hysteresis and lattice parameters are implemented. Remarkably, our study leads to thin-film alloy compositions that have near-zero hysteresis, as determined by resistance measurements. Subsequently, we successfully transfer these thin-film results to bulk materials, and verify their substantially improved functional stability against thermal cycling.

2. Results and Discussion

For the search of thermoelastic SMAs with extremely small thermal hysteresis width, the geometric non-linear theory of martensite (GNLTM)[11–14] has provided successful theoretical guidance.[6] The theory describes several conditions in order for a SMA to show extremely low hysteresis. The first condition, $\det \mathbf{U} = 1$, where $\mathbf{U}$ is the transformation stretch matrix, represents the condition of "no volume change." The second condition, $\lambda_2 = 1$, where $\lambda_1 \geq \lambda_2 \geq \lambda_3$ are the ordered eigenvalues of the transformation stretch matrix $\mathbf{U}$, represents the presence of an invariant plane between austenite and martensite, that is, "a perfectly coherent interface." At such an interface, the energy contributions to the bulk energy through the presence of an elastic transition layer or the interfacial energy of fine arrays of twin bands is eliminated, thus leading to a decrease in the width of the thermal hysteresis (ΔT). Recently, microstructural investigations of $Ti_{50}Ni_{50-x}Pd_x$ alloys by TEM confirmed the existence of twinless martensite at such perfect austenite/martensite interfaces for $Ti_{50}Ni_{39}Pd_{11}$.[15]

Using a combinatorial method, the predicted correlation between λ_2 and ΔT was previously confirmed within the Ti–Ni–Cu system, whereas only a weak correlation between ΔT and volume change ($\det \mathbf{U}$) was found.[6] In view of this experimental evidence and based on investigations of other ternary alloy systems (Ti–Ni–Pd, Ti–Ni–Pt, Ti–Ni–Au), a new theory of hysteresis was recently proposed.[7] This theory is based on the hypothesis that the main energy barrier, leading to hysteresis, arises from the growth of fully developed austenite/martensite interfaces. Thus, it highlights the fundamental importance of the $\lambda_2 = 1$ condition in order to find thermoelastic SMAs with near-zero ΔT. However, to date, no such compositions were found for ternary Ti–Ni based SMAs. Therefore, a further tuning of the lattice parameters by increasing the number of constituent elements, as proposed by James and Zhang,[12] is needed. Specifically, they predicted that certain compositions within the Ti–Ni–Cu–Pd alloy system would exactly fulfill the $\lambda_2 = 1$ condition.[12] This is reasonable, considering that the λ_2 values for Ti–Ni–Cu and Ti–Ni–Pd alloys showing a cubic (B2) to orthorhombic (B19) phase transformation were found to be close to, but slightly smaller or greater, than 1, respectively.[6]

In order to investigate the Ti–Ni–Cu–Pd system, we applied thin-film sputter deposition of quaternary composition spreads[16,17] and high-throughput characterization of the phase-transformation properties (transformation temperatures, ΔT) and lattice parameters of martensite and austenite using temperature-dependent resistance measurements ($R(T)$) and synchrotron X-ray microdiffraction (μXRD(T)), respectively (see Experimental for details).

Figure 1 illustrates the composition variation of the quaternary Ti–Ni–Cu–Pd thin-film composition spread. The variation in Ti content was confined to 47 to 64 at% (Fig. 1a) and the composition

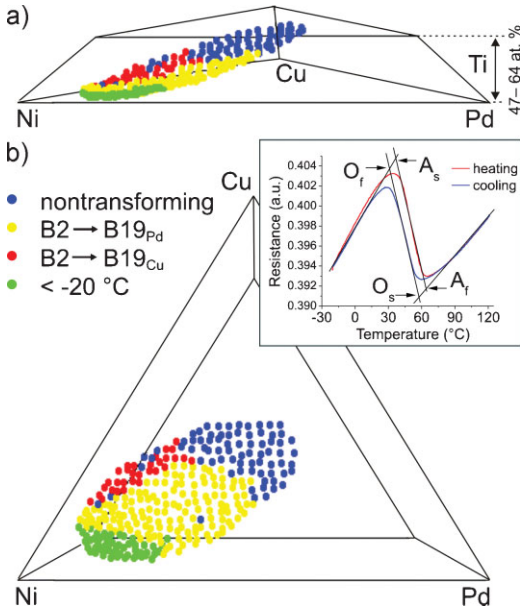

Figure 1. Investigated compositions in the quaternary Ti–Ni–Cu–Pd thin-film continuous composition spread plotted within a) a section of the quaternary composition space, Ti contents: 47–64 at% and b) a projection of the quaternary composition space (tetrahedron) onto a pseudo-ternary Ni–Cu–Pd section. Color coding details are given in the text (visualization by QuaternaryViewer [16]). Inset in b) shows a typical $R(T)$ curve exhibiting a reversible phase transformation. Additionally the phase-transformation temperatures O_s, O_f, A_s, and A_f are indicated as determined by the tangent method.

variations of Ni, Cu, and Pd were adjusted in order to cover the predicted composition region[12] (Fig. 1b). A typical $R(T)$ curve showing a reversible phase transformation is shown in the inset in Figure 1b, where the phase-transformation temperatures A_s, A_f (austenite start and finish), O_s, and O_f (orthorhombic martensite start and finish) as determined by the tangent method, are indicated. The color coding in Figure 1a and b indicates regions with reversible phase transformations having non-linear $R(T)$ curves (red, yellow), and non-transforming regions (blue) having a linear $R(T)$ curves. Compositions, for which the $R(T)$ curves show the presence of a reversible phase transformation starting below –20 °C, the lower bound of the investigated temperature range, are depicted in green. Thus, we show that the upper limit of Ti concentration for the composition region exhibiting reversible phase transformation for quaternary Ti–Ni–Cu–Pd SMAs is 55 at%.

For all compositions showing a reversible phase transformation, the phase-transformation path was found to be from cubic austenite (B2) to orthorhombic martensite ($B19_{Cu}$: red; $B19_{Pd}$: yellow[18]), as confirmed by μXRD(T). Transformation temperatures A_f and O_s, as well as the thermal hysteresis width ($\Delta T = A_f - O_s$) are indicated by color in Figure 2a–c, respectively. For clarity, a projection of the quaternary composition space onto a pseudo-ternary section (Ni–Cu–Pd) is used. For Cu-rich and Pd-poor compositions a clear boundary associated with a pronounced increase in the transformation temperatures is found, indicating a change in the phase-transformation behavior. It is at this boundary, where alloy compositions show near-zero ΔT (as marked in dark blue in Fig. 2c).

A number of compositions are highlighted (red box) in Figure 2c and their corresponding $R(T)$ curves are shown in Figure 3. As the Ni to Pd ratio is varied at fairly constant Ti and Cu contents, a crossover between a S-shaped $R(T)$ curve, characteristic for Ti–Ni–Pd SMAs[19,20] and an inverse S-shaped $R(T)$ curve, characteristic for Ti–Ni–Cu SMAs[21] is observed. Where both characteristic shapes of the $R(T)$ curves merge, alloys with ΔT approaching zero were found. One such composition is $Ti_{50.0}Ni_{34.0}Cu_{11.5}Pd_{4.5}$.

To verify the relationship between ΔT and λ_2 in the Ti–Ni–Cu–Pd system, we calculated λ_2 values by $\lambda_2 = b/\sqrt{2}{}^*a_0$[12] using the lattice parameters of austenite (a_0) and orthorhombic martensite (a, b, c). These were extracted from diffraction patterns obtained by synchrotron μXRD(T) measurements. In the ΔT versus λ_2 plot (Fig. 4a), a strong correlation between ΔT and λ_2 is evident, as depicted by the clear V-shaped distribution of the data. The color code in Figure 4a highlights the fact that alloy compositions with Pd content >> Cu content generally show λ_2 values > 1 (blue), while compositions with Cu content >> Pd content show λ_2 values < 1 (green), which is in agreement with measurements for Ti–Ni–Cu and Ti–Ni–Pd SMAs. The initial data analysis showed that the V-shape distribution was slightly offset (~ −0.003) from $\lambda_2 = 1$ (dashed line) due to thin-film stresses present in the austenitic state (see Experimental and Supporting Information, Fig. 1).

In Figure 4b we plot the present data together with data from our previous investigations of various ternary alloy compositions. Compared to the ternary, we find that the present quaternary compositions, with λ_2 values very close to 1, show a sharp

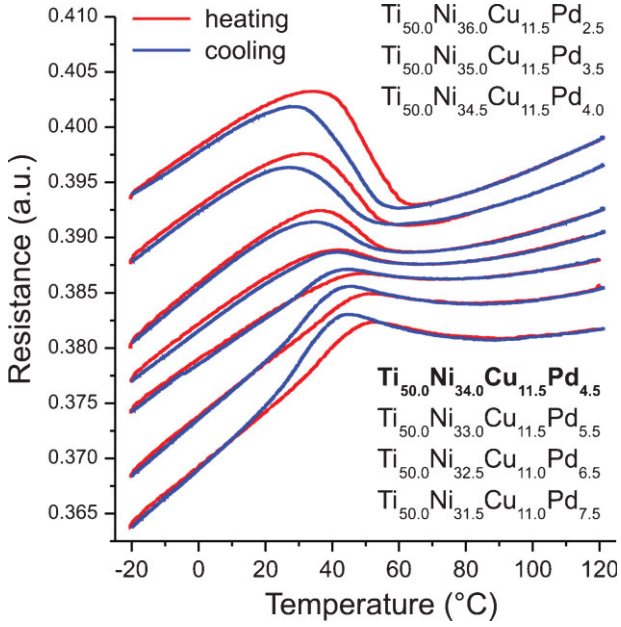

Figure 3. $R(T)$ curves for Ti–Ni–Cu–Pd thin films. The curves are offset for clarity. Compositions are additionally highlighted in Figure 2c.

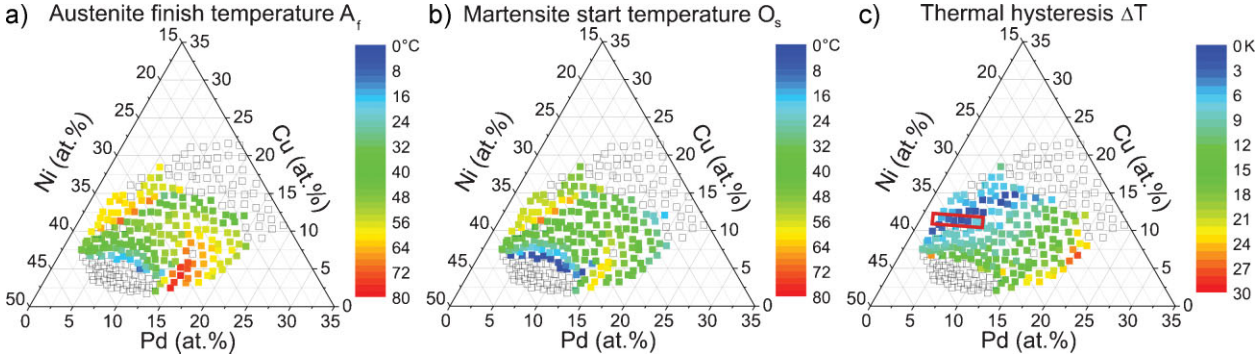

Figure 2. Phase-transformation characteristics for Ti–Ni–Cu–Pd thin films: a) transformation temperatures A_f, b) O_s, and c) $\Delta T = A_f - O_s$ plotted color-coded within the projection of the quaternary composition space (tetrahedron) onto a pseudo-ternary section (Ni–Cu–Pd). Ti content still varies from 47 to 64 at%, as seen in Figure 1a. Red box in (c) highlights compositions, of which the corresponding $R(T)$ curves are shown in Figure 3.

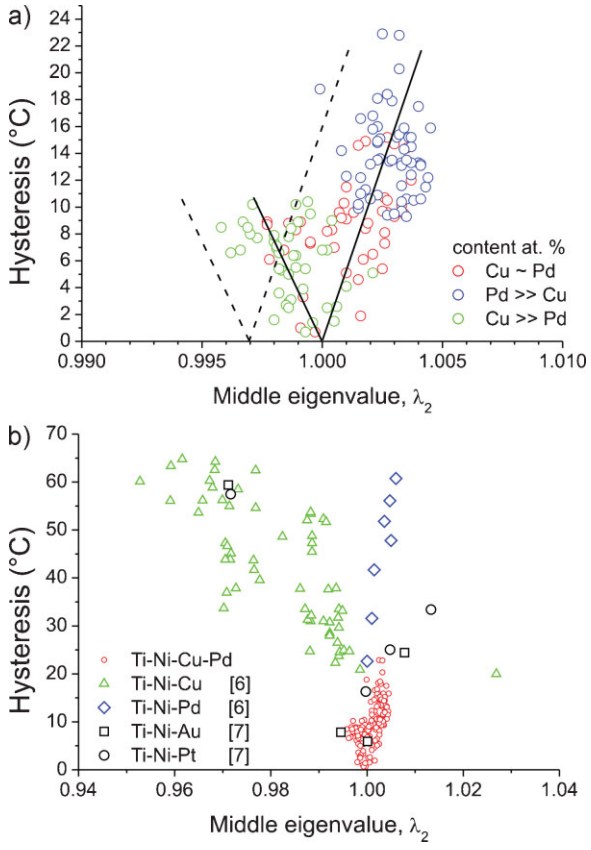

Figure 4. Thermal hysteresis values in Ti–Ni based SMAs. a) ΔT for Ti–Ni–Cu–Pd alloys and b) ternary Ti–Ni–*X* alloys (*X* = Cu [6], Pd [6], Au [7], Pt [7]) plotted against λ_2. The dashed line indicates as-measured values for λ_2, color-coded data points are corrected for residual strain (see Experimental for details). Lines are guides to the eye.

convergence of the thermal hysteresis towards zero for alloy compositions approaching $\lambda_2 = 1$. Despite the fact that a variety of sample preparation methods and measurement techniques were used in the investigation of the different samples, the overall trend of decreasing ΔT values for alloy compositions approaching $\lambda_2 = 1$ is compelling. Other parameters (e.g., elastic modulus, interfacial energy density, and latent heat of transformation) are not expected to vary significantly for the investigated alloys, and thus are concluded to have only a negligible effect on ΔT.[7]

The transformation behavior in the investigated quaternary Ti–Ni–Cu–Pd system is dominated by the Pd content, as evident from the large composition region showing a B2→$B19_{Pd}$ phase transformation (Fig. 1) and the strong dependence of the $R(T)$ characteristic on the Pd content (Figs. 2 and 3). The strong influence of Pd on the transformation characteristics and lattice parameters and thus λ_2 can be rationalized by the substitution behavior of Pd, which is known to occupy Ni sites, irrespectively of concentration,[22] and has a comparatively larger atomic volume. In contrast, Cu atoms show no site preference[22] and have comparable atomic volume to that of Ni. Thus, for additions of Cu, the sensitivity of ΔT to λ_2 is nearly one order of magnitude smaller than that for Pd.[6]

In order to transfer the identified thin-film Ti–Ni–Cu–Pd compositions to bulk, we performed a systematic synthesis of bulk alloys based on the composition–structure–property relationship determined using the combinatorial thin-film approach, that is, the strong correlation of phase-transformation properties on the Ni to Pd ratio, while Ti and Cu contents remain constant (Fig. 3). A direct scale-up of the thin-film compositions is not possible due to the uncertainty associated with the determination of the composition of the transforming phase in the thin film (see Experimental), thin film stresses, and the usually smaller grain sizes in thin films as compared to their bulk counterparts.[23,24] We thus prepared Ti–Ni–Cu–Pd bulk materials by arc-melting with the described systematic compositional variation and characterized their phase-transformation behavior. The most common characterization technique for bulk alloys, differential scanning calorimetry (DSC), was found to be inadequate for characterizing and comparing phase transformations with exceedingly small ΔT, due to the inherent delay of the measurement signal (see Experimental and Supporting Information, Fig. 2).[23]

Thus, we used the temperature-dependent alternating current potential drop method (ACPD) technique, which we have previously established as a reliable method for comparative measurements of transformation temperatures and hysteresis for bulk alloys.[23] For comparison, $Ti_{50}Ni_{50}$ ($\lambda_2 = 0.969$),[25] $Ti_{50}Ni_{35}Cu_{15}$ ($\lambda_2 = 0.995$),[25] and $Ti_{50}Ni_{39}Pd_{11}$ ($\lambda_2 = 1.008$) alloys were also prepared and characterized by the same methods as the quaternary Ti–Ni–Cu–Pd SMAs. Earlier measurements have established both $Ti_{50}Ni_{35}Cu_{15}$ and $Ti_{50}Ni_{39}Pd_{11}$ as the alloys with the lowest λ_2 values within the corresponding ternary system.[25] Figure 5a shows the normalized $R(T)$ curves of the bulk alloys (equally scaled and offset for clarity). These curves confirm the remarkable decrease in ΔT as the alloy compositions approach $\lambda_2 = 1$ and, indeed, immeasurably small or near-zero thermal hysteresis was found for the alloy $Ti_{50.2}Ni_{34.4}Cu_{12.3}Pd_{3.1}$.

The characteristic shapes of the $R(T)$ curves for ternary and quaternary bulk alloys closely resemble those observed for thin films (Fig. 3). The reversible phase transformation for the quaternary $Ti_{50.2}Ni_{34.4}Cu_{12.3}Pd_{3.1}$ alloy was confirmed by temperature-dependent X-ray diffraction (XRD(T)), as shown in Figure 5b. The XRD(T) spectra recorded during heating from 0 to 120 °C show a phase transformation from an orthorhombic martensite ($B19_{Cu}$) to austenite (B2) between 60 and 70 °C and no precipitates. Similarly, the reverse phase transformation was observed to occur during cooling (not shown here). Thus, we have demonstrated the ability to transfer the thin-film results to bulk, based on the composition–structure–property relationship determined using the combinatorial thin film approach.

In order to relate the decrease in ΔT to the functional fatigue characteristics, we investigated the functional stability of $Ti_{50}Ni_{50}$, $Ti_{50}Ni_{35}Cu_{15}$, $Ti_{50}Ni_{39}Pd_{11}$, and $Ti_{50.2}Ni_{34.4}Cu_{12.3}Pd_{3.1}$ by thermal cycling using DSC. Figure 6a–d shows compilations of 20 DSC cycles for the binary and ternary alloys and 80 DSC cycles for $Ti_{50.2}Ni_{34.4}Cu_{12.3}Pd_{3.1}$. Insets highlight the shifting of the DSC curves upon thermal cycling (Fig. 6b–d), which is most clearly visible for the $Ti_{50}Ni_{50}$ alloy (Fig. 6a). The shifting of the transformation temperature during each cycle is associated with an increase in dislocation density (transformation plasticity). Stress fields around the dislocations introduced by thermal cycling

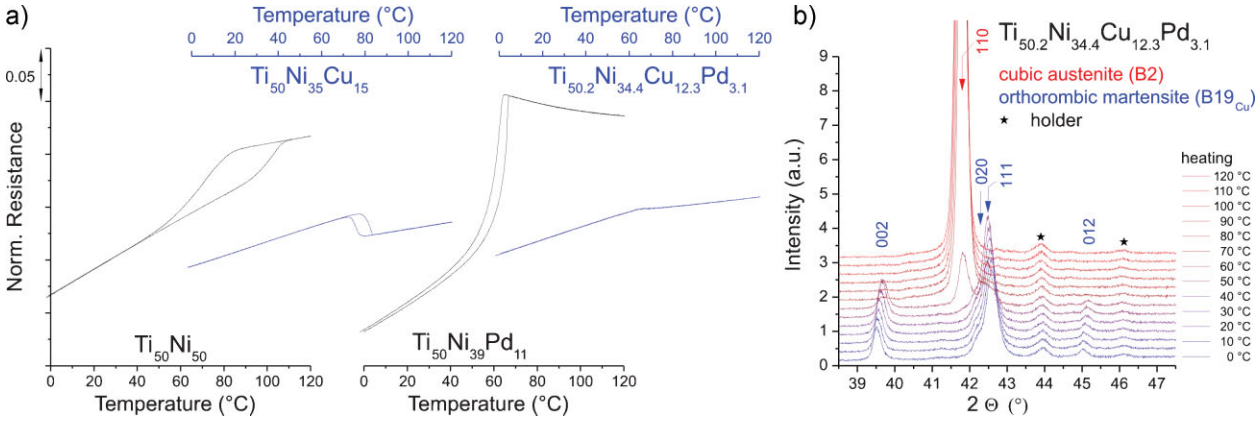

Figure 5. Phase-transformation characteristics of bulk alloys. a) Temperature-dependent ACPD measurements of $Ti_{50}Ni_{50}$, $Ti_{50}Ni_{35}Cu_{15}$, $Ti_{50}Ni_{39}Pd_{11}$, $Ti_{50.2}Ni_{34.4}Cu_{12.3}Pd_{3.1}$, and b) XRD pattern of $Ti_{50.2}Ni_{34.4}Cu_{12.3}Pd_{3.1}$ upon heating from 0 to 120 °C. $R(T)$ curves and spectra are offset for clarity.

impede the elementary transformation processes, thus leading to decreasing transformation temperatures.[1,26] Even though $Ti_{50}Ni_{35}Cu_{15}$ and $Ti_{50}Ni_{39}Pd_{11}$ already show significantly improved functional fatigue as compared to $Ti_{50}Ni_{50}$, an unprecedented functional stability was found for the quaternary near-zero hysteresis alloy $Ti_{50.2}Ni_{34.4}Cu_{12.3}Pd_{3.1}$ alloy. Precipitate hardening, known to be effective in improving the functional fatigue behavior of SMA[26] can be ruled out, since no precipitate phases were detected in the thin films or bulk material using XRD techniques. Furthermore, TEM investigations of ternary $Ti_{50.2}Ni_{30}Cu_{19.8}$ thin films also confirmed that no precipitates are found for the samples annealed at 500 °C for 1 h.[27]

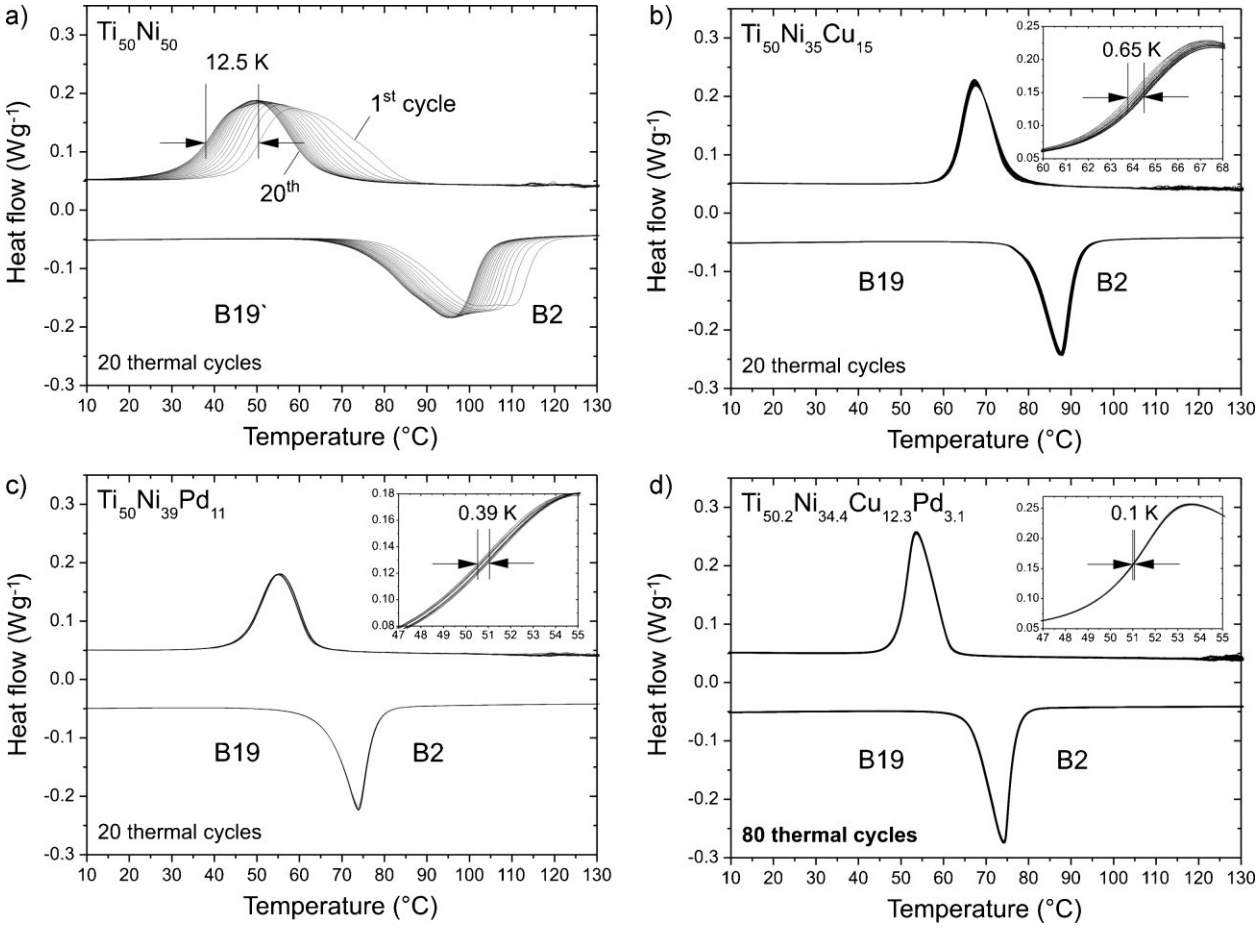

Figure 6. Functional fatigue behavior of bulk alloys. Compilations of 20 DSC cycles are plotted for a) $Ti_{50}Ni_{50}$, b) $Ti_{50}Ni_{35}Cu_{15}$, c) $Ti_{50}Ni_{39}Pd_{11}$, and d) 80 DSC cycles for $Ti_{50.2}Ni_{34.4}Cu_{12.3}Pd_{3.1}$. The insets in (b), (c), and (d) show the shifting of the DSC curves as indicated by the arrows.

3. Conclusions

By extending the thin-film combinatorial methodology to the investigation of quaternary alloys, we identified Ti–Ni–Cu–Pd SMAs with near-zero ΔT as predicted by the GNLTM. We demonstrated the effectiveness of the combinatorial approach in systematically investigating composition–structure–property relationships, which provided the basis for transferring the thin-film results to bulk materials. The determined singular nature of the ΔT versus λ_2 plot entails an exceedingly tight control of composition in order to obtain alloys with minimum hysteresis. By using a resistance-based technique for the characterization of the phase-transformation properties of bulk material, we found a quaternary bulk SMA ($Ti_{50.2}Ni_{34.4}Cu_{12.3}Pd_{3.1}$) that exhibits near-zero thermal hysteresis and unprecedented functional stability. Thus, a critical scientific and practical question of how low one can make the hysteresis by improving the geometric compatibility of two phases has been answered. Other processes, generally believed to contribute to the transformation hysteresis, such as pinning[28] or thermal activation,[7] are therefore concluded to be less critically affecting the hysteresis width of reversible martensitic phase transformations in SMAs. Having potentially solved the perennial problem of functional fatigue, the discovered compositions open up new avenues for SMA applications. More broadly speaking, because of the general nature of the GNLTM, the present findings point to the intriguing possibilities that one can go beyond SMAs and explore its applicability to a wide range of other materials systems where functionalities are also derived from structural phase transformations (e.g., piezoelectric materials). One would dial-in on compositions of such materials to minimize the undesirable hysteresis by tuning the lattice parameters as designed by the theory.

4. Experimental

Thin-film quaternary Ti–Ni–Cu–Pd composition spreads were deposited on 4-in. thermally oxidized (1.5-μm SiO_2) Si wafers (thickness 500 μm) using an ultrahigh-vacuum magnetron sputtering system [17]. Individual layers were sputtered from elemental 4-in. diameter sputtering cathodes. A combination of wedge-type multilayers producing a ternary Ni–Cu–Pd composition spread [21] with intermediate homogenous layers of Ti was applied for the fabrication of a quaternary composition spread. The resulting multilayer structure (total film thickness ~750 nm) was annealed in vacuum at 500 °C for 1 h. The individual compositions of 301 points, evenly distributed over the composition spread wafer (Δx, $\Delta y = 4.5$ mm) were mapped by energy-dispersive X-ray analysis (EDX). However, the overall film composition determined by EDX analysis may deviate from the composition of the transforming phase, since the entire film volume is probed, including surface oxides (TiO, Ti_2O) and the oxygen-stabilized Ti_2Ni interfacial layer at the SiO_2/Si(100) substrate [28]. However, it can be estimated that the composition of the transforming phase will be depleted in Ti and enriched in Cu and Pd as compared to the overall film composition, due to the formation of the Ti-rich interfacial layers, which show limited solubility of Cu and Pd [28,29].

Phase-transformation characteristics of the thin-film composition spread were characterized using temperature-dependent resistance measurements ($R(T)$) in a temperature range from −20 to 120 °C [30]. The phase-transformation temperatures were determined by the tangent method. The crystal structure of thin-film samples was characterized using synchrotron μXRD at the 2-BM beam line of the Advanced Photon Source at Argonne National Laboratory. For this, the wafer was cut into 301 squares (4.5×4.5 mm^2) consistent with the analysis by EDX and $R(T)$. Diffraction measurements were performed at 110 °C (i.e., austenitic state) and at −20 °C (i.e., martensitic state). Measurement times of 200 s per spot were used to obtain sufficient diffracted intensity for a complete lattice parameter analysis of the thin-film samples using an image-plate detector (MAR 345). The beam size was focused to 15×15 μm^2 using a set of 30 Be compound refractive lenses and the photon energy was set to 15 keV. The system was calibrated using a CeO_2 standard (National Institute of Standards and Technology). Lattice parameters were extracted from integrated diffraction patterns and used to calculate the middle eigenvalues λ_2.

The thermal stresses, which arise from the mismatch of the thermal expansion coefficients between substrate and thin films, were evaluated using the $\sin^2\psi$ technique assuming a biaxial stress state [31], which is valid when the film thickness is much smaller than the substrate thickness (as is true in our case). Supporting Information Figure 1 shows contour plots of the angle ψ (angle between the diffracting plane normal and the sample surface normal) versus the d-value (lattice spacing). The diffracted intensity is presented in color code, indicating the stress state of the martensite (left) and austenite (right) phases. For the (020) martensite peak measured at –20 °C, the d-values do not vary with changing ψ angle, indicating the absence of thin-film stresses. This stress relaxation is due to the ability of the martensite to accommodate stresses through reorientation of martensite variants. For the austenite (110) peak measured at 110 °C (above O_s, Fig. 2b), a clear variation of the d-values with ψ angle is evident. By plotting the d-value versus $\sin^2\psi$ (not shown), a linear variation is obtained, and the slope of this variation can be used to calculate the stress directly [31]. An average tensile stress of ~350 MPa was determined, which corresponds closely to the maximum thin-film stresses measured in Ti–Ni–Cu alloys (Ti content: 47–54 at%) using the cantilever deflection method [32]. From the determined stress, σ, the strain, ε, of the thin film was calculated by $\varepsilon = \sigma/E$, where E is the film's biaxial modulus $E_A/(1-\nu)$ [32]. A Young's modulus of austenite, E_A, of 80 GPa and a Poisson ratio, ν, of 0.33 was used for calculation. An average tensile strain of 0.3% was found for the substrate-attached thin film. Thus, the intrinsic austenite lattice parameters are smaller than the measured ones. By applying a correction factor based on the average tensile strain to the measured austenite lattice parameters and recalculating λ_2 values, the thin-film stresses are taken into account. In a previous study on Ti–Ni–Cu thin films, no effect of thin-film stresses on the calculated λ_2 value was found within the experimental error [6]. Therein, the significantly larger variation of λ_2, as compared to this study, may have concealed a systematic shift of the λ_2 values, which is two orders of magnitude smaller than the variation of λ_2 itself.

Bulk samples ($Ti_{50}Ni_{50}$, $Ti_{50}Ni_{35}Cu_{15}$, $Ti_{50}Ni_{39}Pd_{11}$, and Ti–Ni–Cu–Pd) were prepared from pure metals (Ti: > 99.7 mass%; Ni: > 99.98 mass%; Cu: > 99.99 mass%; Pd: > 99.95 mass%) using arc-melting. The binary alloy was remelted ten times, while the ternary and quaternary alloys were remelted fifteen times. After melting, the alloys were sealed separately in evacuated quartz tubes, homogenized at 950 °C for 24 h ($Ti_{50}Ni_{50}$, $Ti_{50}Ni_{35}Cu_{15}$) or at 1000 °C for 24 h ($Ti_{50}Ni_{39}Pd_{11}$, $Ti_{50.2}Ni_{34.4}Cu_{12.3}Pd_{3.1}$) and subsequently water-quenched. The quaternary alloy ($Ti_{50.2}Ni_{34.4}Cu_{12.3}Pd_{3.1}$) was further annealed at 500 °C for 24 h in vacuum in order to exploit the same composition–structure–property relationship as found for the thin-film composition spread annealed at 500 °C for 1 h. ACPD measurements were carried out in order to determine the $R(T)$ characteristics (i.e., phase-transformation temperatures and ΔT) of the bulk alloys [23]. The phase-transformation paths for the bulk alloys were verified by XRD(T) using a PANalytical X'Pert PRO MPD equipped with heating/cooling stage (Anton Paar TTK 450). Functional fatigue of the bulk alloys was evaluated using thermal cycling at a heating/cooling rate of 10 K min^{-1} in a temperature range from −150 to 150 °C using a DSC (DSC 204 F1 Phoenix). Additional DSC measurements for $Ti_{50.2}Ni_{34.4}Cu_{12.3}Pd_{3.1}$ with different heating/cooling rates (1, 2.5, 5, 10, 20 K min^{-1}) were carried out, as shown in Supporting Information Figure 2. The results clearly show that ΔT decreases with decreasing heating/cooling rate, however, the measurements prove to be inadequate to capture near-zero hysteresis values due to the inherent delay of the measurement signal. Thus, we used ACPD measurements for comparison of the near-zero hysteresis behavior of different bulk alloys, as stated above.

Acknowledgements

We thank V. Chevrier and J. R. Dahn for providing the QuaternaryViewer software and would like to acknowledge J. Cui, Ch. Zamponi, M. Yokoyama, E. Quandt, and M. Wuttig for fruitful discussions. This work was supported by the German Research Foundation (DFG) within the collaborative research center "SFB 459" (RZ, BM, MR, JF, GE, AL), the Heisenberg program (AL), the state of North Rhine-Westphalia through the Research Department "Integrity of Small-Scale Systems/High-Temperature Materials" (RZ, GE, AL). M. L. Young is supported by the Alexander von Humboldt Foundation. Use of the Advanced Photon Source was supported by the US Department of Energy, Office of Science, Office of Basic Energy Sciences, under Contract No DE-AC02-06CH11357. Additionally this work was funded by ARO-MURI-W911NF-07-0410, NIH EB 005997 and partially supported by NSF MRSEC DMR 0520471 (RT, IT) and NSF/NNIN (RJ, VS). Supporting Information is available online from Wiley InterScience or from the author.

Received: December 11, 2009
Revised: February 19, 2010
Published online: May 11, 2010

[1] N. B. Morgan, C. M. Friend, *J. Phys. IV* **2001**, *11*, Pr8–325.
[2] J. Perkins, *Metall. Mater. Trans. B* **1973**, *4*, 2709.
[3] D. M. Norfleet, P. M. Sarosi, S. Manchiraju, M. F. X. Wagner, M. D. Uchic, P. M. Anderson, M. J. Mills, *Acta Mater.* **2009**, *57*, 3549.
[4] T. Simon, A. Kröger, C. Somsen, A. Dlouhy, G. Eggeler, *Acta Mater.* **2010**, *58*, 1850.
[5] G. Eggeler, E. Hornbogen, A. Yawny, A. Heckmann, M. Wagner, *Mater. Sci. Eng. A* **2004**, *378*, 24.
[6] J. Cui, Y. S. Chu, O. O. Famodu, Y. Furuya, J. Hattrick-Simpers, R. D. James, A. Ludwig, S. Thienhaus, M. Wuttig, Z. Zhang, I. Takeuchi, *Nat. Mater.* **2006**, *5*, 286.
[7] Z. Zhang, R. D. James, S. Müller, *Acta Mater.* **2009**, *57*, 4332.
[8] J. S. Juan, M. L. No, C. A. Schuh, *Nat. Nanotechnol.* **2009**, *4*, 415.
[9] K. Gall, H. J. Maier, *Acta Mater.* **2002**, *50*, 4643.
[10] C. Grossmann, J. Frenzel, V. Sampath, T. Depka, G. Eggeler, *Metall. Mater. Trans.* **2009**, *11*, 2530.
[11] J. M. Ball, R. D. James, *Phil. Trans. R. Soc. London* **1992**, *338*, 389.
[12] R. D. James, Z. Zhang, in: *Magnetism and Structure in Functional Materials*, 1st ed. (Eds: A. Planes, L. Mañosa, A. Saxena), Springer, Berlin **2005**, 159.
[13] K. Bhattacharya, S. Conti, G. Zanzotto, J. Zimmer, *Nature* **2004**, *428*, 55.
[14] K. Bhattacharya, R. D. James, *Science* **2005**, *307*, 53.
[15] R. Delville, D. Schryvers, Z. Zhang, R. D. James, *Scr. Mater.* **2009**, *60*, 293.
[16] V. Chevrier, J. R. Dahn, *Meas. Sci. Technol.* **2006**, *17*, 1399.
[17] A. Ludwig, R. Zarnetta, S. Hamann, A. Savan, S. Thienhaus, *Int. J. Mater. Res.* **2008**, *99*, 1144.
[18] P. L. Potapov, S. E. Kulkova, A. V. Shelyakov, K. Okutsu, S. Miyazaki, D. Schryvers, *J. Phys. IV* **2003**, *112*, 727.
[19] A. A. Klopotov, V. P. Sivokha, N. M. Matveeva, Y. A. Sazanov, *Russ. Phys. J.* **1993**, *6*, 20.
[20] R. Zarnetta, A. Savan, S. Thienhaus, A. Ludwig, *Appl. Surf. Sci.* **2007**, *254*, 743.
[21] R. Löbel, S. Thienhaus, A. Savan, A. Ludwig, *Mater. Sci. Eng. A* **2008**, *481–482*, 151.
[22] G. Bozzolo, R. D. Noebe, H. O. Mosca, *J. Alloy Compd.* **2005**, *389*, 80.
[23] R. Zarnetta, D. König, C. Zamponi, A. Aghajani, J. Frenzel, G. Eggeler, A. Ludwig, *Acta Mater.* **2009**, *57*, 4169.
[24] B. Winzek, E. Quandt, *Mater. Res. Soc. Symp. Proc.* **2000**, *604*, 117.
[25] Z. Zhang, MS Thesis University of Minnesota, USA **2004**.
[26] S. Miyazaki, Y. Igo, K. Otsuka, *Acta Metall.* **1986**, *34*, 2045.
[27] X. L. Meng, M. Sato, A. Ishida, *Scr. Mater.* **2008**, *59*, 451.
[28] R. Zarnetta, E. Zelaya, G. Eggeler, A. Ludwig, *Scr. Mater.* **2009**, *60*, 352.
[29] R. Hassdorf, J. Feydt, R. Pascal, S. Thienhaus, M. Boese, T. Sterzl, B. Winzek, M. Moske, *Mater. Trans.* **2002**, *43*, 933.
[30] S. Thienhaus, C. Zamponi, H. Rumpf, J. Hattrick-Simpers, I. Takeuchi, A. Ludwig, *Mater. Res. Soc. Symp. Proc.* **2006**, 894:0894-LL06-06.1.
[31] I. C. Noyan, J. B. Cohen, *in Residual Stress*, Springer, New York **1986**, Ch. 5.
[32] P. Krulevitch, A. P. Lee, P. B. Ramsey, J. C. Trevino, J. Hamilton, M. A. Northrup, *J. Microelectromech. Syst.* **1996**, *5*, 270.